**Full Paper**

# FLUID FLOW INDUCED BY AN ELASTIC PLATE IN HEAVING MOTION

May Hlaing Win Khin[a,d]*, Kentaro Kato[b,d], Hyung Jin Sung[c], Shinnosuke Obi[d]

[a]Department of Mechanical Engineering, West Yangon Technological University, Yangon, Myanmar
[b]Linné Flow Centre, Department of Mechanics, Royal Institute of Technology, Stockholm, Sweden.
[c]Department of Mechanical Engineering, Korea Advanced Research Institute of Science and Technology, Daejeon, Korea.
[d]Department of Mechanical Engineering, Keio University, Yokohama, Japan.

## Graphical abstract
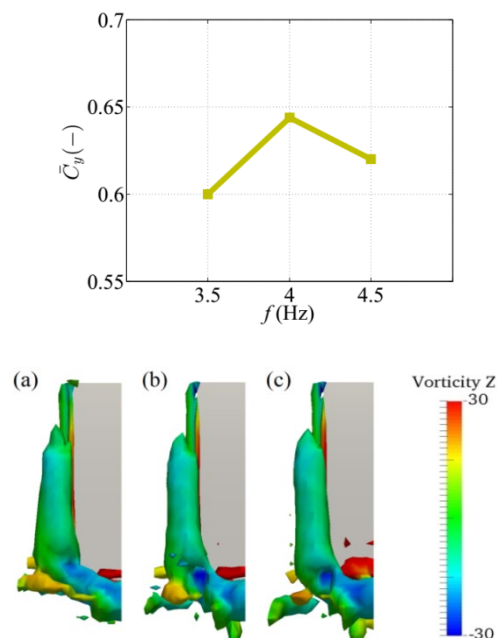
## Abstract

We perform three-dimensional simulations of an elastic plate heaving in a sinusoidal motion with different frequencies to explore the effects of the forcing heaving frequency on the hydrodynamic force generation and flow structures. It is aimed to simulate the motion of a rectangular elastic plate, representing a simplified flexible wing or fin, placed in an open water tank as in a corresponding experimental study. The top edge of the plate oscillates sinusoidally in water at rest. Simulations are conducted for the fluid structure interaction of an elastic plate with a special version of the open-source library C++ OpenFOAM, foam-extend-3.2. The plate oscillates at different heaving frequencies in a range of 3.5 Hz and 4.5 Hz. Experiments are carried out to validate our simulations. The results are in a good agreement with the experiment in terms of the representation of the resonant frequency and the induced hydrodynamic forces. It is found that the hydrodynamic force and propulsive efficiency are mainly affected by the elastic deformation and forcing heaving frequencies. The generated thrust is observed to be significantly enhanced at the resonant frequency, while the propulsive efficiency is increased at the heaving frequency which is greater than the resonant frequency. The results of our simulations point to the importance of resonant flapping frequency for considering the optimal heaving frequency to achieve the best performance and to get the improved thrust force, which are crucial for the locomotion of birds, insects, fishes, flapping-based micro air and underwater vehicles.

*Keywords*: Flexible wing, fluid structure interaction, resonant frequency, thrust force, underwater vehicles

## 1.0 INTRODUCTION

A number of studies on the flow around flapping wings or fins at low Reynolds number have been carried out in recent years [1-10]. Since the flow interaction with flexible flapping wings is complex, there is a need to understand the flow field of flexible structures. Masoud *et al*. [11] numerically studied the aerodynamics induced by flexible wings oscillating at resonance with low Reynolds number. In their work, the flexible wing could produce more lift force than the rigid one at resonant frequency. Vanella *et al*. [12] investigated the effect of flexibility on the aerodynamic performance of flexible wings in a hovering condition. At non-linear resonance, the best aerodynamics performance could be improved by the wing flexibility. Michelin *et al*. [13] conducted numerical analysis on the propulsive performance of a flexible heaving wing in order to examine the effect of flexibility. The mean

thrust maximum occurred at the resonance frequency, at which the amplitude of the trailing edge becomes maximum.

In the work of Spagnolie *et al.* [14], the effect of flexibility in a flapping locomotion was explored experimentally and numerically. The maximum horizontal velocity occurred near the resonant frequency of the flapping wings. Kang *et al.* numerically studied the flexibility effects on the force production and propulsive efficiency of flapping wings [15]. The greater propulsive force was achieved near the resonant flapping, while the maximum propulsive efficiency was not achieved at resonance. An experimental result for the effect of resonant frequency on the wake structure and thrust force was described in the work of Leftwich *et al.* [16]. They employed a passively flexible tail of robotic lamprey in an anguilliform swimming condition and found that the thrust force could be enhanced by the resonant flapping frequency of a flexible tail.

Kato *et al.* experimentally investigated the effect of wing flexibility using different materials of flexible plate [17]. As a representation of flexibility, the forcing frequency relative to the resonance frequency of the plate was selected and the investigations were undertaken at different relative frequencies. It was observed that the induced flow around the plate tip region was affected by the relative frequency. The direction of the induced flow below the plate tip region altered from upward to downward as the forcing frequency exceeded the resonance frequency of the plate. In order to obtain a clear visualization of flow field and generated force induced by the flapping plate, this work need to be studied numerically in details. Although most of numerical simulations had been performed to examine the effect of material flexibility on the flow field and aerodynamic characteristics [18-28], there had been little work that uses fully coupled fluid structure interaction to explore the effect of resonant frequency on the three-dimensional flow structure and corresponding forces [11, 29].

The objective of present study is to get insights into the role of resonant frequency in the hydrodynamic force generation and propulsive efficiency of flapping plate. We performed computational fluid structure interaction analysis following the experimental study by Kato *et al.* [17, 30] in order to examine the flow structure induced by an elastic plate heaving around the resonant frequency. A rectangular elastic plate, which represents a simplified flexible wing or fin, is oscillated with sinusoidal motion in water at rest. We first performed a preliminary simulation to estimate relative amplitude of the plate tip and resonant frequency of the elastic plate for comparison with the experiments. The effects of elastic deformation and heaving frequencies were then investigated by comparing the vortex pattern, hydrodynamic force coefficients and propulsive efficiency.

## 2.0 METHODOLOGY

Computations were conducted with a foam-extend-3.2 version of open-source library C++ OpenFOAM: This version implemented a partitioned solver "fsiFoam" for the strong coupling fluid structure interaction [31]. In this solver, the force and velocity obtained from solving fluid and solid fields are coupled at the fluid structure interface according to the Dirichlet-Neumann procedure. To enforce the equilibrium of the force and velocity at the fluid structure interface, the convergence acceleration with Aitken

relaxation was used in the Gauss-Seidel iteration schemes. Both the fluid and structural equations were discretized based on a finite volume method.

### 2.1 Geometry of Elastic Plate Model

A simplified model of elastic plate is shown in Figure 1. The plate was immersed in water of the tank and clamped at the top edge, which was oscillated sinusoidally in the horizontal direction. The plate had the chord length $C$ of 44 mm, the span length $L$ of 20 mm and the thickness of 1 mm. A heaving motion was imposed on top edge of the elastic plate in the $x$ direction as follows:

$$x_{in} = A_{in} \sin(2\pi\phi) \tag{1}$$

$$\phi = ft \quad (0 < \phi < 1) \tag{2}$$

where $x_{in}$ is the $x$ position of the plate edge or root, $A_{in}$ is the amplitude of the plate root, $\phi$ is the non-dimensional phase, $f$ is the input heaving frequency and $t$ is time.
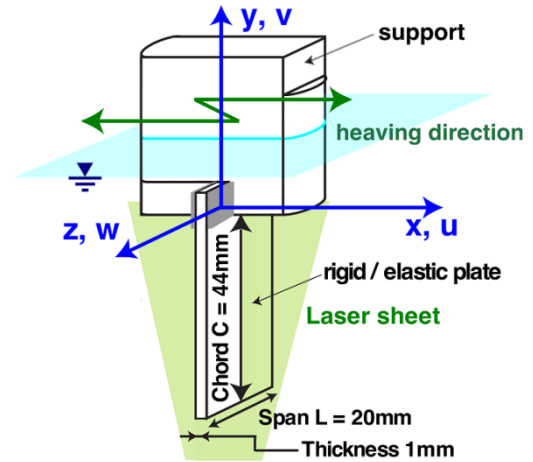


**Figure 1** Elastic plate geometry [17]

### 2.2 Governing Equations

The flow field is governed by incompressible Navier-Stokes equations for viscous flow. Arbitrary Lagrangian-Eulerian method is employed to solve the fluid flow equations on a deforming mesh [32]:

$$\nabla \cdot \boldsymbol{u_f} = 0 \tag{3}$$

$$\frac{\partial \boldsymbol{u_f}}{\partial t} + \left( \boldsymbol{u_f} - \boldsymbol{u_{m,f}} \right) \cdot \nabla \boldsymbol{u_f} = -\frac{\nabla p}{\rho} + \upsilon_f \nabla^2 \boldsymbol{u_f} \tag{4}$$

where $\boldsymbol{u_f}$ and $p$ are the fluid velocity and pressure, $\boldsymbol{u_{m,f}}$ is the mesh velocity, $\rho$ is the fluid density and $\upsilon_f$ is the kinematic viscosity of the fluid. For the solid field, the governing equations of structural solver can be described as follows [33].

$$\rho_s \frac{\partial^2 \boldsymbol{u}}{\partial t^2} = \nabla \cdot \left( \sum \cdot \boldsymbol{F^T} \right) + \rho_s \boldsymbol{f_b} \tag{5}$$

where $u$ is the displacement of the solid, $\rho_s$ is the density of the solid, $\Sigma$ is the second Piola-Kirchhoff stress tensor, $F$ is the deformation gradient tensor and $f_b$ is the resulting body force. The relation for the constitutive equation of a St. Venant-Kirchhoff material and the deformation gradient tensor $F$ is as follows:

$$\Sigma = 2\mu_s G + \lambda_s \text{tr}(G)I \qquad (6)$$

$$G = \frac{1}{2}(F^T.F - I) \qquad (7)$$

$$F = I + (\nabla u)^T \qquad (8)$$

where $\mu_s$ and $\lambda_s$ are Lame constants which are related to Young's modulus and Poisson's ratio of the material, $\Sigma$ is the second Piola-Kirchhoff stress tensor, $G$ is the Green Lagrangian strain tensor and $I$ is the second-order identity tensor.

### 2.2 Computational Domain and Boundary Conditions

The computationl domain is a cuboid with an elastic plate being put in the top center as shown in Figure 2. The fluid domain has dimensions of 150 mm × 200 mm × 20 mm and the solid domain has dimensions of 1 mm × 44 mm × 10 mm in the *x, y* and *z* directions. Both the fluid and solid have no motions at initial conditions. The plate with the same geometry and dimensions was simulated providing the input heaving frequencies of *f* = 3.5, 4.0 and 4.5 Hz. These input heaving frequencies were selected based on the resonant frequency, which lies in the range 3.5 Hz to 4.5 Hz. The heaving amplitude of the plate root was set to $A_{in}$ = 2.9 mm for all heaving frequencies. The working fluid was water with a kinematic viscosity of $\nu_f$ = 1.0 E-6 m$^2$/s and density of $\rho$ = 1.0 E3 kg/m$^3$. The heaving elastic plate is urethane material with a density of $\rho_s$ = 1.25 E3 kg/m$^3$, Poisson's ratio of 0.35 and Young modulus of elasticity of 23.1 MPa.

The "blockMesh" utility was used to generate the mesh in both fluid and solid domains. The fluid domain had 79380 quadrilateral cells while the solid domain had 280 cells. The boundary condition for the front planes of both fluid and solid domain were treated as *symmetryPlane*. For the fluid domain, the *movingWallVelocity* boundary condition was set on the patch named as *interface*, which was interfaced with the plate, for velocity and the *zeroGradient* boundary condition was set for pressure. The boundary conditions on the side, top and bottom patches were utilized with *totalPressure* for pressure and *zeroGradient* for velocity. For the solid domain, the boundary condition on the top surface of the plate was obtained from the imposed heaving motion and *tractionDisplacement* boundary condition was imposed on the interface of the plate surface.

**Table 1** Numerical Schemes

| Type | Used Option |
| --- | --- |
| Time schemes | Euler |
| Gradient schemes | Gauss linear |
| Divergence schemes | Gauss linear |
| Interpolation schemes | Linear |
| Surface normal gradient schemes | SkewCorrected 1 |
| Laplacian schemes | Gauss linear skewCorrected 1 |

The computations were performed on a structured mesh using the "fsiFoam" solver. In this solver, the Pressure Implicit with Split Operators (PISO) algorithm was used for pressure-velocity coupling. The resulting linear system of pressure equation was solved with generalized geometric-algebraic multi-grid (GAMG) algorithm and that of velocity equation was solved with pre-conditioned bi-stab conjugate Gradient (PBiCG) algorithm. The details of numerical schemes applied for discretization are presented in Table 1. The time step was set to 0.01 s and each simulation was conducted for 6 s to ensure the quasi-steady state. The computational time was 9 hours on a PC equipped with Intel®Core™ i5-5257U CPU 2.70GHz × 4 processor.
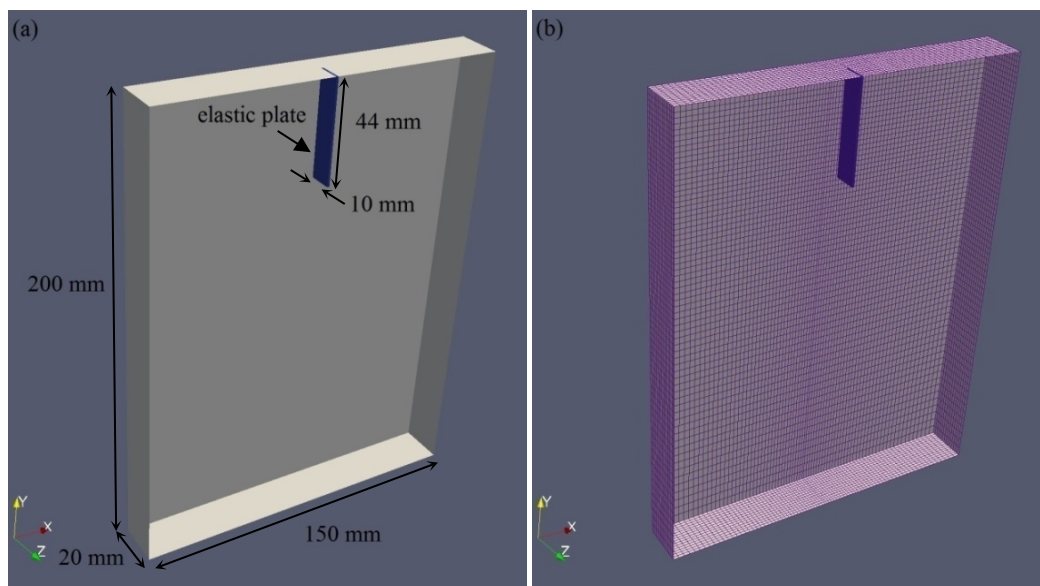


**Figure 2** (a) Schematic view of the computational domain, (b) Structured grid generation. The origin of coordinate is the top center of the plate

## 3.0 RESULTS AND DISCUSSION

### 3.1 Plate Deformation and Validation

As a preliminary simulation, the deformation of the elastic plate is observed using different input heaving frequencies in a range from 3.5 to 4.5 Hz. The resonance frequency $f_n$ of the plate is compared with the measurements [17]. The resulting time histories of the plate tip displacement $x_{out}$ for different heaving frequencies are shown in Figure 3. Dividing the amplitude of the plate tip $A_{out}$ by that of the plate root $A_{in}$ results in a non-dimensional amplitude of the plate tip, from which the resonance frequency of the plate is computed.

Table 2 shows the magnitude of the plate root amplitude $A_{in}$, that of the plate tip amplitude $A_{out}$ and non-dimensional amplitude of the plate tip $A_{out}/A_{in}$ for three cases corresponding to different input heaving frequencies of $f$ = 3.5, 4.0 and 4.5 Hz. The calculations are done after four heaving cycles, where the periodicity of plate tip's motion is achieved in all cases. It is found that the plate has the highest value of relative amplitude of the plate tip at $f$ = 4.0 Hz and we take this frequency as a resonant frequency.

In comparison with the experimental data [17], we find a good agreement with respect to the resonant frequency of the elastic plate, although the magnitude of the plate tip amplitude computed by the current simulations is somewhat larger than that computed by the experiments. Since the experimental data of plate tip amplitude reported in the work of Kato *et al.* [17] were understimated due to the measurement method, there may be discrepancies between the results. The simulation results of relative amplitude of the plate tip are about 0.3 larger than the experimental results. Figure 4 shows a comparison of relative amplitude of the plate tip between the experiments and simulations.
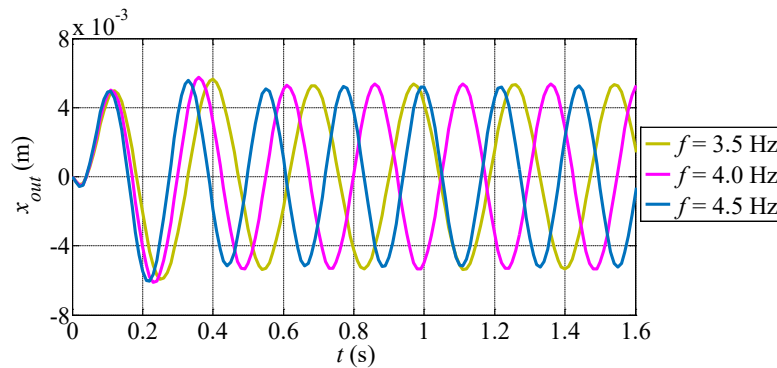
**Table 2** Results of Non-dimensional Relative Amplitude

| Material | $f$ (Hz) | $A_{in}$ (mm) | $A_{out}$ (mm) | $A_{out}/A_{in}$ (-) |
|---|---|---|---|---|
| Urethane | 3.5 | 2.9 | 5.28 | 1.82 |
| Urethane | 4.0 | 2.9 | 5.37 | 1.85 |
| Urethane | 4.5 | 2.9 | 5.25 | 1.81 |



**Figure 3** Time history of the plate tip displacement $x_{out}$ for different heaving frequencies $f$
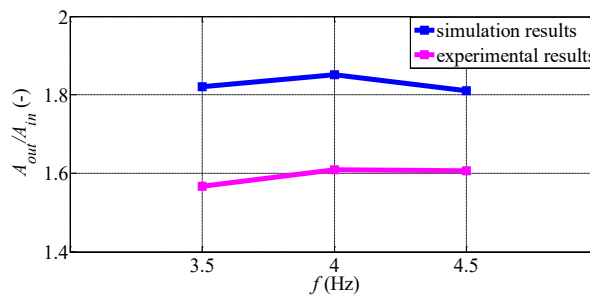


**Figure 4** Comparison of the relative amplitude of the plate tip

### 3.2 Hydrodynamic Forces and Propulsive Efficiency

To estimate the enhancement of hydrodynamic forces and propulsive efficiency induced by the resonance heaving frequency, the instantaneous and time-averaged hydrodynamic force coefficients of the heaving elastic plate are examined for different heaving frequencies. The horizontal and vertical force coefficients of the plate in the $x$ and $y$ directions, $C_x$ and $C_y$, are calculated using the force coefficient's function tool provided in

OpenFOAM. The instantaneous horizontal and vertical force coefficients, $C_x$ and $C_y$ are given by as follows:

$$C_x = \frac{2F_x}{\rho a U^2} \tag{9}$$

$$C_y = \frac{2F_y}{\rho a U^2} \tag{10}$$

where $F_x$ and $F_y$ are the instantaneous horizontal and vertical forces acting on the plate, $\rho$ is the fluid density, $a$ is the reference area of plate and $U$ is the reference velocity. The reference area of the plate is $a = LC$, where $L$ is the span length of the plate and $C$ is the chord length of the plate. The reference velocity $U$ is taken as the maximum heaving velocity of the plate root, $U = 2\pi f A_{in}$, as there is no free stream velocity. The power coefficient of the heaving plate is calculated using the following equation:

$$C_p = \frac{2P}{\rho a U^3} \qquad (11)$$

where $P$ is the instantaneous power input required to initiate the motion of the plate. The instantaneous power input is calculated from the product of instantaneous horizontal forces $F_x$ and the heaving velocities of the plate root:

$$P(t) = -F_x(t)\dot{x}_{in}(t) \qquad (12)$$

The propulsive efficiency is given by:

$$\eta = \frac{\bar{C}_y}{\bar{C}_p} \qquad (13)$$

where $\bar{C}_y$ and $\bar{C}_p$ are time-averaged values over a heaving period, obtained by integrating the values of $C_y$ and $C_p$ with respect to time.
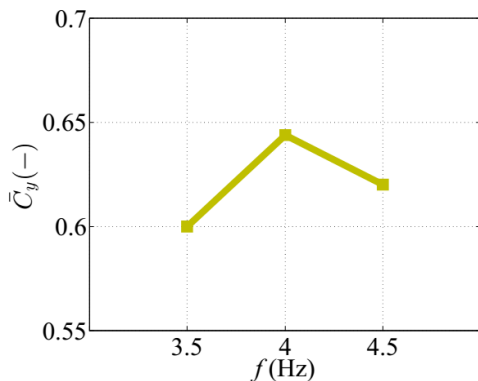


**Figure 5** Time-averaged vertical force coefficients

The time-averaged vertical force coefficients and power coefficients are computed for all heaving frequencies. Figure 5 shows the time-averaged vertical force coefficients of the elastic plate as a function of the heaving frequency. The instantaneous force coefficients are averaged over 10 heaving cycles to get time-averaged force coefficients. As expected, the heaving at various frequencies governs the deformation of the plate tip and significantly affects the vertical force coefficients $C_y$. An optimal frequency is obtained at which the maximum $C_y$ is observed. It is found that the mean vertical force coefficients increase significantly at the resonance frequency of $f = 4.0$ Hz, where the maximum relative amplitude of the plate tip occurs. From Figures 4 and 5, the mean vertical force coefficients $\bar{C}_y$ become higher as the relative amplitude of the plate tip becomes larger. This obviously shows that the thrust force is greatly affected by the resonant heaving frequency since the vertical force coefficients $C_y$ are equivalent to the thrust force coefficients.

On the other hand, Figure 6(a) illustrates that the power coefficient decreases as the plate oscillates at the higher heaving frequency. This indicates that the higher heaving frequency reduces the input power required to initiate the motion of the plate. As a result, the propulsive efficiency $\eta$ increases with the increase of the heaving frequency as shown in Figure 6(b). The value of $\eta$ increases gradually from 0.10 to 0.11 for the heaving frequency of 3.5 and 4.0 Hz, while it increases considerably from 0.11 to 0.125 for the heaving frequency of 4.0 and 4.5 Hz. This may be attributed to the mean power coefficients of the plate heaving at $f = 4.5$ Hz, which is obviously smaller than that of the plate heaving at $f = 4.0$ Hz in Figure 6(a).
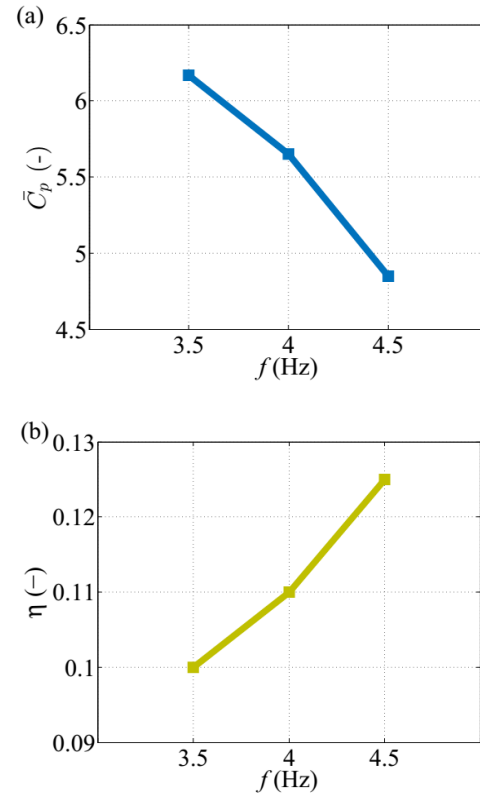


**Figure 6** (a) Time-averaged power coefficient and (b) Propulsive efficiency

Figure 7(a) shows the non-dimensional plate tip displacement $x_{out}/A_{in}$ as a function of the plate root phase $\phi$ to find the characteristics of force coefficients for all cases. The resulting instantaneous vertical and horizontal force coefficients, $C_y$ and $C_x$, at a periodic steady state during one heaving cycle are shown in Figure 7(b) and 7(c). Since the two vortices are periodically generated around the plate tip in one heaving cycle, there exist two distinct peaks in $C_y$ as shown in Figure 7(b). The two peaks are obviously generated in all cases and the plate produces a slightly negative force coefficient around the reversal phase.

Another significant difference is observed in the production of $C_x$ as shown in Figure 7(c). The positive and negative values of $C_x$ are produced alternatively as the motion of the plate alternates in the positive and negative $x$ directions as shown in Figure 7(a) and 7(c). The positive and negative peaks of $C_x$ are generated around the end of each half cycle and the profiles of $C_x$ are similar as that of the plate tip displacement. The time-averaged horizontal force coefficient $C_x$ is zero due to the symmetric heaving motion with

respect to the *y*-axis and no net horizontal forces are generated in all cases. Unlike the oscillations of vertical force coefficients $C_y$, the highest heaving frequency has the smallest oscillation of $C_x$ among the three cases. The fluctuations of $C_x$ become lower as the

heaving frequency becomes higher. This seems to be less power consumption required for heaving the plate during one cycle, resulting in the higher propulsive efficiency.
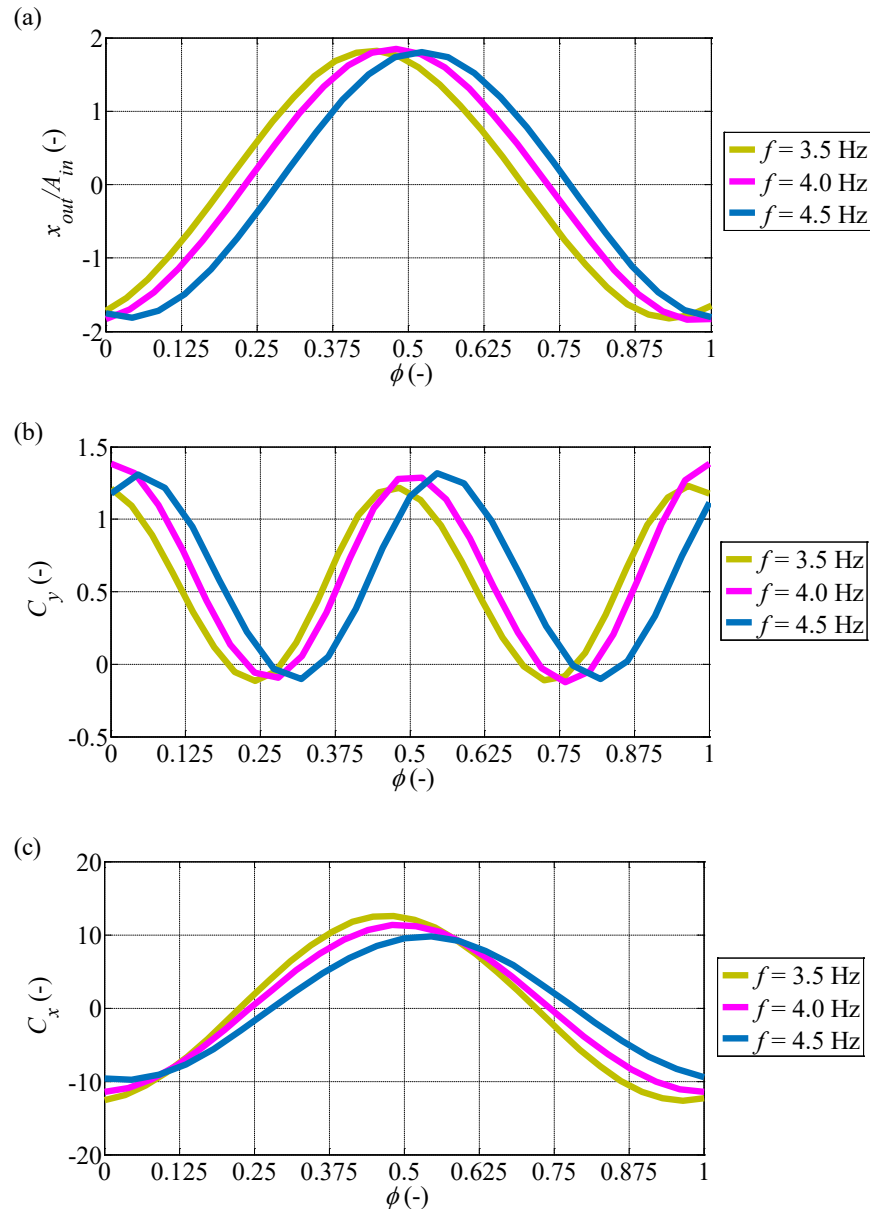
(a)



(b)



(c)



**Figure 7** (a) Non-dimensional plate tip displacement $x_{out}/A_{in}$ (b) Instantaneous vertical force coefficients $C_y$ and (c) Instantaneous horizontal force coefficients $C_x$

### 3.3 Momentum Flow Analysis around the Heaving Plate

To further clarify the flow field induced by the heaving plate, a three-dimensional control volume analysis is used to evaluate the vertical momentum flux, which is related with the generation of thrust force. A control volume ($|x/C| \leq 0.68$, $-1.68 \leq y/C \leq 0$, $z/C \leq 0.27$) is defined around the plate as shown Figure 8(a). Based on the momentum equation, the vertical momentum flux through the control surface can be expressed as [17];

$$F_{yu} = \rho \int_{cs} v(\boldsymbol{V} . \boldsymbol{n}) dA \qquad (14)$$

where $F_{yu}$ is the instantaneous momentum flux through the control surface, $\rho$ is the fluid density, $v$ is the vertical velocity component and $\boldsymbol{n}$ is the outward unit normal vector on the control surface. The time-averaged vertical momentum flux $\bar{F}_{yu}$ can be obtained by averaging the instantaneous vertical momentum flux over a heaving period. The time-averaged vertical momentum flux

$\bar{F}_{yu}$ acting on the control volume is shown in Figure 8(b). $\bar{F}_{yu}$ illustrates a correlation with the generation of thrust force mentioned above. The maximum negative value of $\bar{F}_{yu}$ is observed in the resonant case, in which the maximum of thrust force is observed.
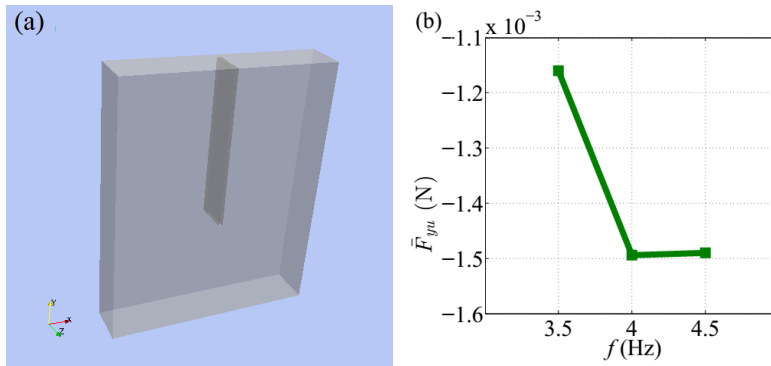


**Figure 8** (a) Schematic view of the control volume surrounding the plate (the origin of coordinate is a top center of the plate) and (b) Time-averaged vertical momentum flux

### 3.4 Vortex Patterns

The vortex evolutions from the plate during a half heaving cycle are illustrated for the case of $f$ = 4.0 Hz as the perspective and left side views in Figures 9(a) and 9(b). The vortex structures around the plate are visualized using iso-surfaces of the instantaneous Q criterion (Q=30), colored by the spanwise vorticity Z. The vortex developed along the vertical edge of the plate is termed a leading-edge vortex (LEV) and the vortex along the horizontal edge on the lower part of the plate is termed a tip vortex (TV).
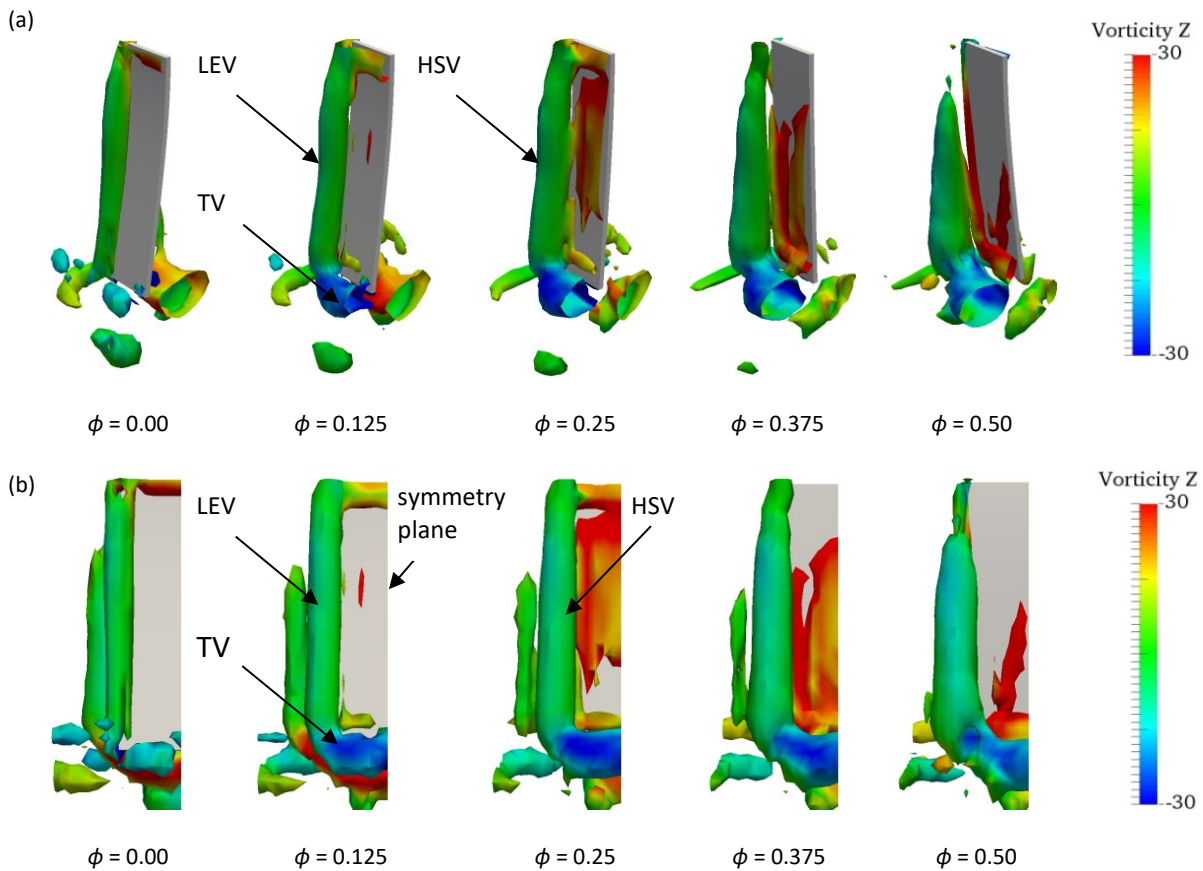


**Figure 9** Iso-surface of the instantaneous Q-criterion (Q=30) around the plate heaving with the frequency $f$ = 4 Hz for half heaving cycle; (a) perspective view and (b) left side view. (Only half of the HSV is seen since the other half plane is symmetric.)

During the first half cycle, from $\phi$ = 0.0 to $\phi$ = 0.50, the plate root is moving to the right from its center position and then reversing its motion to its center position. In the range from $\phi$ = 0.0 to $\phi$ = 0.25, the plate root velocity decreases and becomes zero at $\phi$ = 0.25. As the plate moves to the right, the generation process of a horseshoe-shaped vortex (HSV) is observed behind the plate, around the left surface. HSV is formed from the connecting of LEV with TV. Only half of HSV can be seen in Figure 9(b) because the other half plane is symmetric. A LEV first emerges from the plate edge, and then a TV is formed along the lower edge of the plate and connects the LEV, which forms a horseshoe pattern of vortex around the plate edge as shown in Figure 9(b). As the motion of the plate continues, the size of HSV becomes enlarged by staying attached to the plate.

From $\phi$ = 0.25 to $\phi$ = 0.50, during the plate root's reversal motion to its center position, the velocity of the plate root increases from zero to the maximum. As the translational velocity of the plate root increases, the LEV begins to detach from the upper surface of the plate while the LEV on the lower part of the plate remains attached to the plate. The detached LEV moves toward the lower part of the plate and merges with the TV, which leads to the enlargement of TV. The extension process of TV takes place until the plate tip reverses its direction of motion. In this case, the motion of the plate tip is delayed due to deformation. At $\phi$ = 0.5, we can see that the LEV is firstly moving downward along the left surface of the plate, and the TV is increasing in size. After a half heaving cycle, the HSV gradually decays as a new HSV is developed on the other side of the plate in the following half cycle.

In the second half cycle, the plate root is moving to the left and then back to the center position. Since the vertical flow is symmetric between $\phi$ = 0.0 to 0.50 and $\phi$ = 0.50 to 1.0, similar generation and decaying processes of HSV are observed on the right surface of the plate.
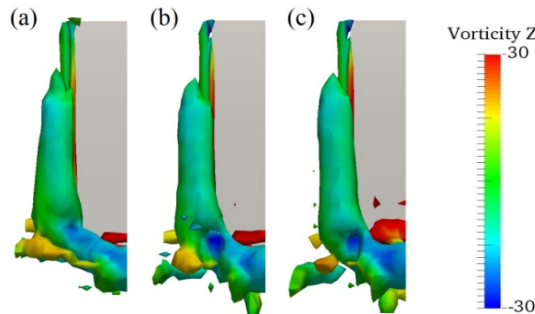


**Figure 10** Iso-surface of the instantaneous Q-criterion (Q=30) around the plate for various heaving frequencies; (a) $f$ = 3.5 Hz (b) $f$ = 4.0 Hz and (c) $f$ = 4.5 Hz

In Figure 10, the vortex structures around the plate at each phase, where the maximum force coefficients happen, are shown for all cases. The HSV around the plate heaving with different frequencies are almost the same. A slight difference in the pattern of LEV and TV can be observed. The first observation is that the plate with lower heaving frequency has the largest LEV among all cases, which leads to the highest power consumption and consequently lowest power efficiency. Another observation is that a resonance case has more uniform and larger TV developed along the most of span length when compared to other cases, which correlates with the higher thrust force production. A significant difference can be seen for $f$ = 3.5 Hz, in which the TV becomes weaker from mid-span to outer part of the plate as shown in

Figure 10(a). These differences in TV seem to be affected by the plate tip amplitude.

Figures 11 shows instantaneous spanwise vorticity contours in the mid-span plane of the heaving plate. The negative and positive vortices are shed alternatively from the plate tip during one heaving cycle as in two dimensions. This type of vortex pattern is a thrust generating type, known as a reverse von Karman vortex, consistent with the results of Kato *et al*. [17]. From these figures, the vortex shedding from the elastic plate heaving with different frequencies is almost similar.
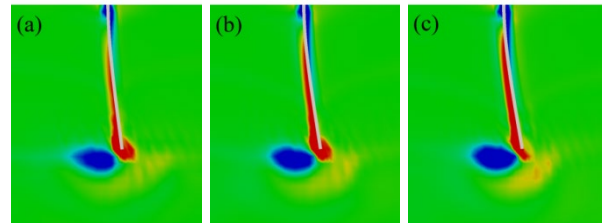


**Figure 11** The spanwise vorticity contours in the mid-span plane of the plate; (a) $f$ = 3.5 Hz (b) $f$ = 4.0 Hz and (c) $f$ = 4.5 Hz

## 4.0 CONCLUSION

Three-dimensional simulations for fluid-structure interaction have been performed using the C++ library OpenFOAM, foam-extend-3.2 version. An elastic plate oscillates in a sinusoidal motion with various heaving frequencies in water at rest. The input heaving amplitude is kept constant in all cases. The deformation of the elastic plate is examined for different heaving frequencies. The normalized amplitude shows a maximum at a heaving frequency which is a resonant frequency of the plate. The simulation results are in good agreement with the experiments. We then compare the flow structure and corresponding hydrodynamics forces for all frequency ranges. It is found that the heaving motion creates a symmetric flow field generating two HSV on each side of the plate within one heaving cycle. Although the generated vortex patterns are nearly the same in all cases, a significant difference is observed in the hydrodynamics force production. The vertical force coefficients are affected by the elastic deformation while the horizontal force coefficients by the heaving frequency. The higher vertical force coefficients are related to the maximum amplitude of the plate tip, induced by the resonance heaving frequency. The horizontal force coefficients keep decreasing with increasing the heaving frequency. Consequently, the maximum propulsive efficiency is enhanced at the higher heaving frequency beyond the resonance. The optimal heaving frequency to achieve the best performance and to get the improved thrust force should be taken into account in combination with a resonant heaving frequency.

## References

[1]     Yin, B., and Luo, H. 2010. Effect of Wing Inertia on Hovering Performance of Flexible Flapping Wings. *Physics of Fluids*. 22(11): 11902,1-10 DOI : 10.1063/1.3499739

[2]     Minotti, F., O. 2011. Determination of the Instantaneous Forces on Flapping Wings from a Localized Fluid Velocity Field. *Physics of Fluids*. 23(11). DOI : 10.1063/1.3659496

[3]     Lee, J., S., Seo, I., S., and Lee, S., H. 2015. Propulsion Velocity of a Flapping Wing at Low Reynolds Number. *Journal of Fluids and Structures*. 54: 422-439. DOI: 10.1016/j.jfluidstructs.2014.12.002

[4]     Wu, D., Yeo, K., S., and Lim, T., T. 2014. A Numerical Study on the Free Hovering Flight of a Model Insect at Low Reynolds Number. *Computers & Fluids*. 103: 234-261. DOI: 10.1016/j.compfluid.2014.07.030

[5]     Broering, T., M., and Lian, Y. 2015. Numerical Study of Tandem Flapping Wing Aerodynamics in Both Two and Three Dimensions. *Computers & Fluids*. 115: 124-139. DOI: 10.1016/j.compfluid.2015.04.003

[6]     Altememe, A., Myers, O., J., and Hall, A. 2019. Preliminary Design and Computational Fluid Dynamic Analysis of Flapping Wing of Micro Aerial Vehicle for Low Reynolds Numbers Regime. *International Journal of Aeronautics and Aerospace Engineering*. 1(2): 36-45. DOI: 10.18689/ijae-1000106

[7]     Hua, Z., Y., Hui, H., J., and Huat, L., K. 2013. Numeric Simulation on the Performance of an Undulating Fin in the Wake of a Periodic Oscillating Plate. *International Journal of Advanced Robotic Systems*. 10(10): 1-12. DOI :  10.5772/56439

[8]     Dong, H., Mittal, R., and Najjar, F., M. 2006. Wake Topology and Hydrodynamic Performance of Low-Aspect-Ratio Flapping Foils. *Journal of Fluid Mechanics*. 566: 309-343. DOI : 10.1017/S002211200600190X

[9]     Li, G., Müller, U., K., Leeuwen, J., L., and Liu, H. 2012. Body Dynamics and Hydrodynamics of Swimming Fish Larvae: a Computational Study. *The Journal of Experimental Biology*. 215: 4015-4033. DOI : 10.1242/jeb.071837

[10]    Suryadi, A., and Obi, S. 2012. An Attempt to Evaluate Pressure Force on a Flapping Rigid Plate Using Velocity Data of PIV Measurements. *ASEAN Engineering Journal Part A*. 1(1): 30-44.

[11]    Masoud, H., and Alexeev, A. 2012. Efficient Flapping Flight Using Flexible Wings Oscillating at Resonance. *Natural Locomotion in Fluids and on Surfaces*. 155: 235-245.

[12]    Vanella, M., Fitzgerald, T., Preidikman, S., Balaras, E., and Balachandran, B. 2009. Influence of Flexibility on the Aerodynamic Performance of a Hovering Wing. *The Journal of Experimental Biology*. 212(1): 95-105. DOI : 10.1242/jeb.016428

[13]    Michelin, S., and Smith, S., G., L. 2009. Resonance and Propulsion Performance of a Heaving Flexible Wing. *Physics of Fluids*. 21(7): 071902, 1-15. DOI : 10.1063/1.3177356

[14]    Spagnolie, S., E., Moret, L., Shelley, M., J., and Zhang, J. 2010. Surprising Behaviors in Flapping Locomotion with Passive Pitching. *Physics of Fluids*. 22(4): 041903,1-20 DOI : 10.1063/1.3383215

[15]    Kang, C., K., Aono, H., Cesnik, C., E., S., and Shyy, W. 2011. Effects of Flexibility on the Aerodynamic Performance of Flapping Wings. *Journal of Fluid Mechanics*. 689: 32-74. DOI : 10.1017/jfm.2011.428

[16]    Leftwich, M., C., Tytell, E., D., Cohen, A., H., and Smits, A., J. 2012. Wake Structures Behind a Swimming Robotic Lamprey with a Passively Flexible Tail. *The Journal of Experimental Biology*. 215(3): 416-425. DOI: 10.1242/jeb.061440

[17]    Kato, K. 2010. *PIV Measurements in Complex Flows Bounded by Deforming Surface*. Thesis (Master), Keio University, Yokohama, Japan.

[18]    Zhu, X., He, G., and Zhang, X. 2014. Numerical Study on Hydrodynamic Effect of Flexibility in a Self-Propelled Plunging Foil. *Computer δ Fluids*. 97: 1-20.

[19]    Lee, J., S., and Lee, S., H. 2013. Fluid–Structure Interaction for the Propulsive Velocity of a Flapping Flexible Plate at Low Reynolds Number. *Computer δ Fluids*. 71: 348-374,

[20]    Qi, D., Liu, Y., Shyy, W., and Aono, H. 2010. Simulations of Dynamics of Plunge and Pitch of a Three-Dimensional Flexible Wing in a Low Reynolds Number Flow. *Physics of Fluids*. 22(9): 1-20. DOI: 10.1063/1.3481786

[21]    Ho, S., Nassef, H., Pornsinsirirak, N., Tai, Y.C., and Ho, C.M. 2003. Unsteady Aerodynamics and Flow Control for Flapping Wing Flyers. *Progress in Aerospace Science*. 39(8): 635-681. DOI: 10.1016/j.paerosci.2003.04.001

[22]    Eldredge, J., D., Toomey, J., and Medina, A. 2010. On the Roles of Chord-Wise Flexibility in a Flapping Wing with Hovering Kinematics. *Journal of Fluid Mechanics*. 659: 94-115. DOI: 10.1017/S0022112010002363

[23]    Hua, R., N., Zhu, L., and Lu, X.Y. 2013. Locomotion of a Flapping Flexible Plate. *Physics of Fluids*. 25(12): 1-17. DOI: 10.1063/1.4832857

[24]    Lee, K., B., Kim, J., H., and Kim, C. 2011. Aerodynamic Effects of Structural Flexibility in Two-Dimensional Insect Flapping Flight. *Journal Of Aircraft*. 48(3): 894-909. DOI: 10.2514/1.C031115

[25]    Wu, J., Shu, C., Zhao, N., and Tian, F., B. 2015. Numerical Study on the Power Extraction Performance of a Flapping Foil with a Flexible Tail. *Physics Of Fluids*. 27(1): 1-15. DOI: 10.1063/1.4905537

[26]    Jaworski, J., W., and Gordnier, R., E. 2015. Thrust Augmentation of Flapping Airfoils in Low Reynolds Number Flow Using a Flexible Membrane. *Journal of Fluids and Structures*. 52: 199-209. DOI: 10.1016/j.jfluidstructs.2014.08.010

[27]    Nakata, T., and Liu, H. 2012. A Fluid–Structure Interaction Model of Insect Flight with Flexible Wings. *Journal of Computational Physics*. 231(4): 1822-1847. DOI: 10.1016/j.jcp.2011.11.005

[28]    Cheng, X., and Lan, S. 2015. Effects of Chordwise Flexibility on the Aerodynamic Performance of a 3D Flapping Wing. *Journal of Bionic Engineering*. 12(3): 432-442. DOI: 10.1016/S1672-6529(14)60134-7

[29]    Masoud, H., and Alexeev, A. 2010. Resonance of Flexible Flapping Wings at Low Reynolds Number. *Physical Review E*. 81: 056304, 1-5 DOI: 10.1103/PhysRevE.81.056304

[30]    Lee, I., and Sung, H., J. 1999. Development of an Array of Pressure Sensors with PVDF Film. *Experiments in Fluids*. 26: 27-35.

[31]    Tukovi, Z., Cardiff, P., Karac, A., Jasak, H., and Ivankovic, A. 2014. OpenFOAM Library for Fluid Structure Interaction. *9th OpenFOAM Workshop,* Zagreb, Croatia.

[32]    Donea, J., Huerta, A., Ponthot, J.-Ph. and Rodriguez-Ferran, A. 2004. Arbitrary Lagrangian–Eulerian Methods. *Encyclopedia of Computational Mechanics*. 1: 413-437.

[33]    Tuković, Ž., Karač, A., Cardiff, P., Jasak, H., and Ivanković, A. 2018. OpenFOAM Finite Volume Solver for Fluid-Solid Interaction. *Transactions of Famena*. 1-31. DOI: 10.21278/TOF.42301